Journal of Theoretical Biology 370 (2015) 81–92

Contents lists available at ScienceDirect

Journal of Theoretical Biology

journal homepage: www.elsevier.com/locate/yjtbi

Modelling the movement of interacting cell populations: A moment dynamics approach

Stuart T. Johnston [a,b,*], Matthew J. Simpson [a,b], Ruth E. Baker [c]

[a] School of Mathematical Sciences, Queensland University of Technology (QUT), Brisbane, Australia
[b] Institute of Health and Biomedical Innovation, QUT, Brisbane, Australia
[c] Mathematical Institute, University of Oxford, Oxford, United Kingdom

HIGHLIGHTS

- New moment dynamics model to describe the movement of interacting cell populations.
- Moment dynamics model applied to mimic two different cell biology experiments.
- Moment dynamics predictions outperform traditional mean-field PDE descriptions.
- Provide guidance regarding situations where the moment dynamics model is required.

ARTICLE INFO

Article history:
Received 28 November 2014
Received in revised form
16 January 2015
Accepted 20 January 2015
Available online 30 January 2015

Keywords:
Cell motility
Cell proliferation
Cancer
Wound healing
Moment closure

ABSTRACT

Mathematical models describing the movement of multiple interacting subpopulations are relevant to many biological and ecological processes. Standard mean-field partial differential equation descriptions of these processes suffer from the limitation that they implicitly neglect to incorporate the impact of spatial correlations and clustering. To overcome this, we derive a moment dynamics description of a discrete stochastic process which describes the spreading of distinct interacting subpopulations. In particular, we motivate our model by mimicking the geometry of two typical cell biology experiments. Comparing the performance of the moment dynamics model with a traditional mean-field model confirms that the moment dynamics approach always outperforms the traditional mean-field approach. To provide more general insight we summarise the performance of the moment dynamics model and the traditional mean-field model over a wide range of parameter regimes. These results help distinguish between those situations where spatial correlation effects are sufficiently strong, such that a moment dynamics model is required, from other situations where spatial correlation effects are sufficiently weak, such that a traditional mean-field model is adequate.

1. Introduction

Biological and ecological processes often involve moving fronts of interacting subpopulations. For example, in a biological setting, malignant spreading occurs when tumour cells interact with, and move through, the stroma (Bhowmick and Moses, 2005; De Wever and Mareel, 2003; Gatenby et al., 2006; Li et al., 2003). In an ecological setting, the spreading of an invasive species involves moving fronts, that, in some cases, is coupled with a retreating front of that species' prey (Hastings et al., 2005; Phillips et al., 2007; Skellam, 1951).

Fig. 1 shows images of two different types of cell biology experiments involving moving fronts of interacting subpopulations. Fig. 1(a)–(c) shows images of a co-culture scratch assay (Oberringer et al., 2007). This assay is constructed such that initially we have two subpopulations present in a certain region of the domain that is adjacent to a vacant region. As time proceeds, the two subpopulations spread into the vacant space. The image in Fig. 1(c) indicates that one of the subpopulations is clustered, whereas the other subpopulation is more evenly distributed. The image in Fig. 1(d) shows a subpopulation of initially confined melanoma cells that are spreading into a surrounding subpopulation of fibroblast cells (Li et al., 2003). These images demonstrate that collective cell spreading processes can involve moving fronts of interacting subpopulations. Given the importance of collective cell spreading processes to a range of biological applications, including wound healing and malignant spreading, it is relevant for us to develop robust mathematical and computational tools that can

* Corresponding author at: School of Mathematical Sciences, Queensland University of Technology (QUT), Brisbane, Australia.
E-mail address: s17.johnston@qut.edu.au (S.T. Johnston).

http://dx.doi.org/10.1016/j.jtbi.2015.01.025

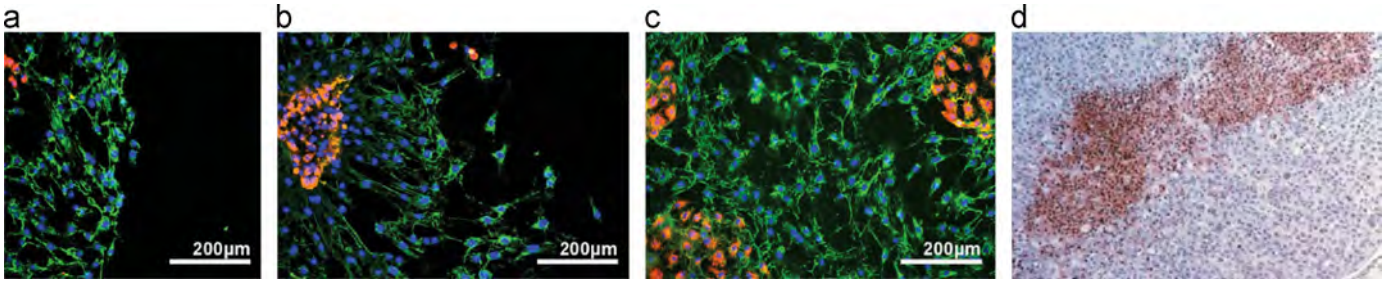

Fig. 1. Co-culture scratch assay containing human dermal microvascular endothelial cells (red) and human dermal fibroblasts (green) at (a) 0 hours, (b) 24 hours and (c) 48 hours. Adapted from Oberringer et al. (2007). (d) Human fibroblasts (blue) and TGF-β1 transduced 451Lu melanoma cells (brown), 19 days after subcutaneous injection into immunodeficient mice. Adapted from Li et al. (2003). (For interpretation of the references to colour in this figure caption, the reader is referred to the web version of this paper.)

accurately describe the motion of these kinds of multispecies moving front problems.

Previous mathematical modelling of problems involving moving fronts of multiple interacting subpopulations have typically involved studying systems of reaction–diffusion partial differential equations (PDEs) (Gatenby and Gawlinski, 1996; Painter and Sherratt, 2003; Sherratt, 2000; Simpson et al., 2007a,b; Smallbone et al., 2005). For example, Sherratt (2000) considers a two-species model of tumour growth. In this model, the movement of the tumour cell subpopulation, $v(x,t)$, is inhibited by the stroma subpopulation, $u(x,t)$. Cell proliferation is also influenced by crowding, since the rate of proliferation is a decreasing function of the total cell density, $u(x,t)+v(x,t)$ (Sherratt, 2000). More generally, Painter and Sherratt (2003) suggest that the motion of interacting cell subpopulations depends on the gradient of each particular species' density, as well as the gradient of the total cell density. Focusing specifically on tumour invasion, Gatenby and Gawlinski (1996) propose a three-species model, where the density of normal tissue decreases due to an excess concentration of H^+ ions. Smallbone et al. (2005) extend the Gatenby and Gawlinski three-species model by including a necrotic core within the tumour, which is more consistent with biological observations. However, while these models provide valuable insight into the interaction of multiple cell subpopulations, they are limited in two ways. First, each of these PDE models relies on invoking a mean-field assumption. That is, these models implicitly assume that individuals in an underlying stochastic process interact at a rate that is proportional to the average density (Grima, 2008). This assumption amounts to the neglect of any spatial structure present in the subpopulations (Law and Dieckmann, 2000). Second, these PDE models describe population-level behaviour, and do not explicitly consider individual-level information that could be relevant when dealing with certain types of experimental data (Simpson et al., 2013).

Instead of working directly with PDEs, mean-field descriptions of collective cell behaviour have been derived from discrete individual-level models (Binder and Landman, 2009; Codling et al., 2008; Fernando et al., 2010; Khain et al., 2012; Simpson et al., 2009, 2010). These discrete models, which can also incorporate crowding (Chowdhury et al., 2005), can be identified with corresponding mean-field continuum PDE models that aim to describe the average behaviour of the underlying stochastic process. Using this kind of approach gives us access to both discrete individual-level information as well as continuum population-level information. For example, to model the migration of adhesive glioma cells, Khain et al. (2012) derive a mean-field PDE description of a discrete process which incorporates cell motility, cell-to-cell adhesion and cell proliferation. However, while the relationship between the averaged discrete data and the solution of the corresponding mean-field PDE description is useful in certain circumstances, it is well-known that the assumptions invoked when deriving mean-field PDE descriptions are inappropriate in certain parameter regimes, due to spatial correlations between the occupancy of lattice sites (Baker and Simpson, 2010; Johnston et al., 2012; Simpson and Baker, 2011). The impact of spatial correlation is relevant when we consider patchy or clustered distributions of cells, such as in Fig. 1(b) and (c). Baker and Simpson (2010) partly address this issue by developing a moment dynamics model that approximately incorporates the effect of spatial correlation. Markham et al. (2013) extend this work, but focus on problems where the initial distribution of cells is spatially uniform, meaning that the modelling and computational tools developed by Markham et al. (2013) are not suitable for studying the motion of moving fronts of various interacting subpopulations.

In this work we consider a discrete lattice-based model for describing the motion of a population of cells where the total population is composed of distinct, interacting subpopulations. To understand how our work builds on previous methods of analysis, we derive a standard mean-field description of the discrete model and demonstrate that, in certain parameter regimes, the mean-field model does not describe the averaged discrete behaviour. By considering the dynamics of the occupancy of lattice pairs, we derive one- and two-dimensional moment dynamics descriptions that incorporate an approximate description of the spatial correlation present in the system. Motivated by the geometry of the two typical cell biology experiments in Fig. 1, we apply our model to two case studies. The first case study is relevant to co-culture scratch assays and the second case study is relevant to the invasion of one subpopulation into another subpopulation, thereby mimicking tumour invasion processes. Through these case studies we demonstrate that our moment dynamics model provides a significantly more accurate description of the averaged discrete model behaviour. Finally, we discuss our results and outline directions for future work.

2. Methods

2.1. Discrete model

We consider a lattice-based random walk model where each lattice site may be occupied by, at most, one agent (Chowdhury et al., 2005). The model is presented for situations where there are two subpopulations, denoted by superscripts G and B, and we note that the framework could be extended to include a larger number of subpopulations if required. The superscripts G and B correspond to the colour scheme in our figures where results relating to the G subpopulation are given in green and results relating to the B subpopulation are given in blue. The discrete process takes place on a one-dimensional lattice, with lattice spacing Δ, where each site is indexed $i \in [1, X]$. Agents on the lattice undergo movement, proliferation and death events at rates P_m^G, P_p^G, P_d^G and P_m^B, P_p^B, P_d^B per unit time, for subpopulations G and B, respectively. During a potential motility event, an agent at site i attempts to move to site $i \pm 1$, with the target site chosen with equal probability. This potential event will be successful only if the target site is vacant. A proliferative agent at site i attempts to place a daughter

agent at site $i \pm 1$, with the target site chosen with equal probability. This event will only be successful if the target site is vacant. Agent death occurs by simply removing an agent from the lattice. For all results presented in this work, we apply periodic boundary conditions. However, in practice, we only consider initial conditions and timescales such that the effects of the boundary conditions at $i=1$ and $i=X$ are unimportant.

For the two-dimensional discrete model, we define a square two-dimensional lattice, with lattice spacing Δ, where each lattice site is indexed (i,j), where $i \in [1,X]$ and $j \in [1,Y]$. A motile agent at (i,j) will attempt to step to site $(i \pm 1, j)$ or $(i, j \pm 1)$, with the target site chosen with equal probability. Similarly, a proliferative agent at (i,j) will attempt to deposit a daughter agent at site $(i \pm 1, j)$ or $(i, j \pm 1)$, with the target site chosen with equal probability. Since the model is an exclusion process, any potential motility or proliferation event that would place an agent on an occupied site is aborted. Agent death occurs by removing an agent from the lattice. While we do not explicitly consider extending this model to a three-dimensional lattice, it is straightforward to perform discrete simulations on a three dimensional lattice (Baker and Simpson, 2010).

We use the Gillespie (1977) algorithm to generate sample paths from the discrete model. An individual realisation of the Gillespie algorithm results in the binary lattice occupancy, $\underline{C}_i^k$, at each site i. To obtain averaged density information we perform M identically prepared realisations of the discrete algorithm and calculate the average lattice occupancy $C_i^k = \langle \underline{C}_i^k \rangle$, which represents the probability that lattice site i is occupied by an agent of subpopulation $k \in \{G, B\}$.

2.2. One-dimensional mean-field approximation

To derive a mean-field description of the discrete model we consider a discrete conservation statement describing the rate of change of the occupancy status of site i. Accounting for all possible motility, proliferation and death events we obtain

$$\frac{dC_i^k}{dt} = \frac{P_m^k}{2}\left[C_{i-1}^k \Phi_i + C_{i+1}^k \Phi_i - C_i^k \Phi_{i-1} - C_i^k \Phi_{i+1}\right] + \frac{P_p^k}{2}\left[C_{i-1}^k \Phi_i + C_{i+1}^k \Phi_i\right] - P_d^k C_i^k, \quad (1)$$

for subpopulation $k \in \{G, B\}$, where $\Phi_i = 1 - \sum_K C_i^K$ is the probability that site i is vacant. Since we interpret the product of site occupation probabilities in Eq. (1) as a net transition probability (Johnston et al., 2012), we explicitly assume that the occupancy status of lattice sites are independent, which is equivalent to neglecting the correlations in occupancy between lattice sites. Extending this kind of mean-field conservation statement to apply to our two-dimensional discrete model is straightforward, and the details are given in the supplementary material document. Standard mean-field descriptions of our discrete model, given by Eq. (1), can be re-written as a PDE description. To see this we expand the $C_{i \pm 1}^k$ terms in Eq. (1) in a Taylor series about site i, neglecting terms of $\mathcal{O}(\Delta^3)$ and smaller. After identifying C_i^k with a continuous function $C^k(x,t)$, we can re-write the resulting expression as a reaction–diffusion PDE for $C^k(x,t)$ (Simpson et al., 2014).

2.3. One-dimensional moment dynamics approximation

Instead of treating products of site occupation probabilities as independent quantities, we now consider the time evolution of the relevant n-point distribution functions, $\rho^{(n)}$ (Baker and Simpson, 2010). The one-point distribution function is given by $\rho^{(1)}(\sigma_i)$, where σ_i denotes the state of site i and can be interpreted as the probability that site i is in state $\sigma \in \{0, A^G, A^B\}$. We note that the possible states of site i are (i) A_i^G, which indicates that site i is occupied by an agent from subpopulation G, (ii) A_i^B, which indicates that site i is occupied by an agent from subpopulation B, and (iii) 0_i, which indicates that site i is vacant (Baker and Simpson, 2010). The evolution of the one-point distribution function for subpopulation k can be described by accounting for all possible motility, proliferation and death events,

$$\frac{d\rho^{(1)}(A_i^k)}{dt} = \frac{P_m^k}{2}\left[\rho^{(2)}(A_{i-1}^k, 0_i) + \rho^{(2)}(A_{i+1}^k, 0_i) - \rho^{(2)}(A_i^k, 0_{i-1}) - \rho^{(2)}(A_i^k, 0_{i+1})\right] + \frac{P_p^k}{2}\left[\rho^{(2)}(A_{i-1}^k, 0_i) + \rho^{(2)}(A_{i+1}^k, 0_i)\right] - P_d^k \rho^{(1)}(A_i^k). \quad (2)$$

The evolution of the one-point distribution functions depends on the two-point distribution functions, which, in this case, means that the evolution of the occupancy status of individual lattice sites depends on the occupancy of nearest-neighbour lattice pairs. For example, the average occupancy of site i increases due to the probability that site i is unoccupied and site $i-1$ is occupied by subpopulation k. We denote this probability, without the assumption that the occupancies of sites i and $i-1$ are uncorrelated, by $\rho^{(2)}(A_{i-1}^k, 0_i)$. To measure the correlation between lattice sites i and m, separated by distance $r\Delta = (m-i)\Delta$, we use the correlation function (Baker and Simpson, 2010)

$$F_i^{a,b}(r\Delta) = \frac{\rho^{(2)}(\sigma_i, \sigma_m)}{\rho^{(1)}(\sigma_i)\rho^{(1)}(\sigma_m)}, \quad (3)$$

where a denotes the state of site i and b denotes the state of site m. We note that $F_i^{a,b}(r\Delta)$ depends on time. However, for notational convenience, we do not explicitly include this dependence in our notation. Employing the relationship (Baker and Simpson, 2010)

$$\rho^{(1)}(\sigma_i) = \sum_{\sigma_m} \rho^{(2)}(\sigma_i, \sigma_m), \quad (4)$$

we rewrite Eq. (2) in terms of the correlation functions. Here, for the specific case where we consider two subpopulations, G and B, we obtain

$$\frac{dC_i^G}{dt} = \frac{P_m^G}{2}\Big[C_{i-1}^G + C_{i+1}^G - 2C_i^G + C_i^B\left\{2C_i^G - C_{i-1}^G F_{i-1}^{G,B}(\Delta) - C_{i+1}^G F_i^{B,G}(\Delta)\right\} - C_i^G\left\{2C_i^B - C_{i-1}^B F_{i-1}^{B,G}(\Delta) - C_{i+1}^B F_i^{G,B}(\Delta)\right\}\Big] + \frac{P_p^G}{2}\Big[C_{i-1}^G\left\{1 - C_i^G F_{i-1}^{G,G}(\Delta) - C_i^B F_{i-1}^{G,B}(\Delta)\right\} + C_{i+1}^G\left\{1 - C_i^G F_i^{G,G}(\Delta) - C_i^B F_i^{B,G}(\Delta)\right\}\Big] - P_d^G C_i^G. \quad (5)$$

Note that if the lattice sites are uncorrelated and hence $F_i^{a,b}(r\Delta) \equiv 1$, Eq. (5) is equivalent to Eq. (1). This simplification emphasises that the key difference between the moment dynamics description and the standard mean-field description is in the way that the two approaches deal with the role of spatial correlation effects. We also note that interchanging G and B in Eq. (5) allows us to write down a similar expression for dC_i^B/dt.

To solve Eq. (5) and the corresponding expression for dC_i^B/dt, we must develop a model for the evolution of $F_i^{G,G}(\Delta)$, $F_i^{B,B}(\Delta)$, $F_i^{G,B}(\Delta)$ and $F_i^{B,G}(\Delta)$. To achieve this we consider the evolution of the relevant two-point distribution functions by considering how potential motility, proliferation and death events alter each two-point distribution function. Here we present details for the lattice pair $(i, i+1)$, where both sites are occupied by subpopulation G. The evolution of the corresponding two-point distribution function is given by

$$\frac{d\rho^{(2)}(A_i^G, A_{i+1}^G)}{dt} = \frac{P_m^G}{2}\Big[\rho^{(3)}(A_{i-1}^G, 0_i, A_{i+1}^G) + \rho^{(3)}(A_i^G, 0_{i+1}, A_{i+2}^G) - \rho^{(3)}(0_{i-1}, A_i^G, A_{i+1}^G) - \rho^{(3)}(A_i^G, A_{i+1}^G, 0_{i+2})\Big] + \frac{P_p^G}{2}\Big[\rho^{(3)}(A_{i-1}^G, 0_i, A_{i+1}^G) + \rho^{(3)}(A_i^G, 0_{i+1}, A_{i+2}^G)\Big] - 2P_d^G \rho^{(2)}(A_i^G, A_{i+1}^G). \quad (6)$$

In general, the evolution of the n-point distribution function depends on the $(n+1)$-point distribution function. This results in a system of equations, the size of which is equivalent to the number of lattice sites, that describe the evolution of the n-point distribution functions. The large number of lattice sites makes this system of equations algebraically intractable, so to make progress we truncate the system using a moment closure approximation (Baker and Simpson, 2010). While several different types of moment closure approximations are available in the literature (Law and Dieckmann, 2000), our previous experience with these kinds of models indicates that the Kirkwood superposition approximation (KSA) (Singer, 2004) is a good option. Therefore, we apply the KSA

$$\rho^{(3)}(\sigma_i,\sigma_j,\sigma_k)=\frac{\rho^{(2)}(\sigma_i,\sigma_j)\rho^{(2)}(\sigma_i,\sigma_k)\rho^{(2)}(\sigma_j,\sigma_k)}{\rho^{(1)}(\sigma_i)\rho^{(1)}(\sigma_j)\rho^{(1)}(\sigma_k)}, \tag{7}$$

to re-write the three-point distribution functions in Eq. (6) in terms of two-point distribution functions. After using the KSA, we rewrite Eq. (6) in terms of the correlation functions to obtain

$$\begin{aligned}\frac{\mathrm{d}F_i^{G,G}(\Delta)}{\mathrm{d}t}=&-F_i^{G,G}(\Delta)\left[\frac{1}{C_i^G}\frac{\mathrm{d}C_i^G}{\mathrm{d}t}+\frac{1}{C_{i+1}^G}\frac{\mathrm{d}C_{i+1}^G}{\mathrm{d}t}\right]\\&+\frac{P_m^G}{2}\left[\frac{C_{i-1}^G}{C_i^G}F_{i-1}^{G,G}(2\Delta)+\frac{C_{i+2}^G}{C_{i+1}^G}F_i^{G,G}(2\Delta)-2F_L^{G,G}(\Delta)\right.\\&+F_i^{G,G}(\Delta)\left\{C_{i-1}^BF_{i-1}^{B,G}(\Delta)F_{i-1}^{B,G}(2\Delta)+C_{i+2}^BF_i^{G,B}(2\Delta)F_{i+1}^{G,B}(\Delta)\right\}\\&-\frac{C_{i+1}^BC_{i+2}^G}{C_{i+1}^G}F_i^{G,B}(\Delta)F_i^{G,G}(2\Delta)F_{i+1}^{B,G}(\Delta)\\&\left.-\frac{C_{i-1}^GC_i^B}{C_i^G}F_{i-1}^{G,B}(\Delta)F_{i-1}^{G,G}(2\Delta)F_i^{B,G}(\Delta)\right]\\&+\frac{P_p^G}{2}\left[\frac{1}{C_i^G}+\frac{1}{C_{i+1}^G}-2F_i^{G,G}(\Delta)-\frac{C_i^B}{C_i^G}F_i^{B,G}(\Delta)-\frac{C_{i+1}^B}{C_{i+1}^G}F_i^{G,B}(\Delta)\right.\\&+\frac{C_{i-1}^GF_{i-1}^{G,G}(2\Delta)}{C_i^G\left(1-C_i^G-C_i^B\right)}\left\{1-C_i^GF_{i-1}^{G,G}(\Delta)-C_i^BF_{i-1}^{G,B}(\Delta)\right\}\\&\times\left\{1-C_i^GF_i^{G,G}(\Delta)-C_i^BF_i^{B,G}(\Delta)\right\}\\&\left.+\frac{C_{i+2}^GF_i^{G,G}(2\Delta)}{C_{i+1}^G\left(1-C_{i+1}^G-C_{i+1}^B\right)}\left\{1-C_{i+1}^GF_i^{G,G}(\Delta)-C_{i+1}^BF_i^{G,B}(\Delta)\right\}\right.\\&\left.\times\left\{1-C_{i+1}^GF_{i+1}^{G,G}(\Delta)-C_{i+1}^BF_{i+1}^{B,G}(\Delta)\right\}\right]-2P_d^GF_i^{G,G}(\Delta).\end{aligned} \tag{8}$$

We observe that the right-hand side of Eq. (8) is undefined where either $C_i^G=0$ or $C_i^G+C_i^B=1$ and we discuss the subsequent method of solution for the system of correlation functions in the supplementary material document.

Eq. (8) shows that the evolution of nearest-neighbour correlation functions, $F_i^{G,G}(\Delta)$, depends on the next nearest-neighbour correlation function at $r\Delta=2\Delta$. Therefore, to make progress we must derive expressions for non-nearest-neighbour correlation functions. To do this we consider the evolution of the correlation function for an arbitrary lattice pair, separated by distance $r\Delta$, and the equations governing the evolution of the correlation function for $r\Delta>\Delta$ that are provided in the supplementary material document. For ease of computation we assume that we have some maximum correlation distance for which, when $r\Delta>r_{\max}\Delta$, we have $F_i^{a,b}(r\Delta)\equiv 1$ (Baker and Simpson, 2010). This means that the occupancy status of lattice sites that are sufficiently far apart are uncorrelated. For all one-dimensional results presented in this document we set $r_{\max}=100$ whereas for all two-dimensional results we set $r_{\max}=5$, and we find that the results of our moment dynamics model are insensitive to further increases in $r_{\max}$. The complete system of governing equations for the one- and two-dimensional correlation functions are given in the supplementary material document.

3. Results

To investigate how the moment dynamics model performs relative to the traditional mean-field model, described by Eq. (1), we now consider two case studies motivated by the experiments illustrated in Fig. 1. To compare the performance of the mean-field and moment dynamics models, we calculate

$$E=\frac{1}{X}\left[\sum_{i=1}^{X}\left(\hat{C}_i^k-C_i^k\right)^2\right]^{1/2}, \tag{9}$$

where X is the number of lattice sites, $\hat{C}_i^k$ is the average density of subpopulation k calculated using a large number of identically prepared realisations of the discrete model and C_i^k is the associated solution of the relevant continuum model. In particular, the discrepancy between the averaged discrete results and the traditional mean-field model is denoted E_{MF}, whereas the discrepancy between the averaged discrete results and the moment dynamics model is denoted E_{MD}. In all cases we solve the governing system of coupled ordinary differential equations using Matlab's `ode45` function, which implements an adaptive fourth order Runge–Kutta method (Shampine and Reichelt, 1997).

3.1. Case study 1: co-culture scratch assay

3.1.1. One-dimensional co-culture scratch assay

Co-culture scratch assays involve growing two cell cultures on a culture plate, performing a scratch to reveal a vacant region and observing how the population of cells then spreads in to the initially vacant region (Oberringer et al., 2007; Walter et al., 2010). While the scratch assay shown in Fig. 1(a)–(c) focuses on spreading in one direction, we consider an initial condition which leads to spreading in two directions:

$$C_i^G(0)=C_i^B(0)=\begin{cases}\epsilon, & 1\le i<i_1,\\ C_0, & i_1\le i<i_2,\\ \epsilon, & i_2\le i\le X,\end{cases} \tag{10}$$

where $\epsilon\ll 1$ to allow for the possibility of some material remaining after the scratch has been made. This initial condition corresponds to both subpopulations being placed, evenly distributed, at the same density, in the region $i_1<i<i_2$. Since the cells are located at random we have $F_i^{a,b}(r)\equiv 1$ at $t=0$.

Representative snapshots from the discrete model at $t=0$, $t=100$ and $t=200$ are presented in Fig. 2(a)–(c), respectively. While the discrete model is one-dimensional, we show 20 identically prepared realisations of the model adjacent to each other in Fig. 2(a)–(c). Reporting the results of the stochastic model in this way gives us a visual indication of the degree of stochasticity in the model. Comparing the spatial distributions of agents at $t=100$ and $t=200$ indicates that the more motile blue subpopulation spreads further from the initial condition than the less motile green subpopulation.

The corresponding averaged density profiles, obtained by considering a large number of identically prepared realisations from the discrete model, are superimposed on the relevant solutions of the mean-field and moment dynamics model for both subpopulations in Fig. 2(d)–(e), respectively, at $t=100$. We immediately observe that the traditional mean-field model predicts qualitatively different behaviour to the averaged discrete model. To demonstrate this we plot the difference between the density of the two subpopulations, $D_i=C_i^B-C_i^G$, in Fig. 2(f). For the averaged discrete density data D_i is predominantly non-negative, whereas the traditional mean-field approach predicts that $D_i<0$ for a significant portion of the domain.

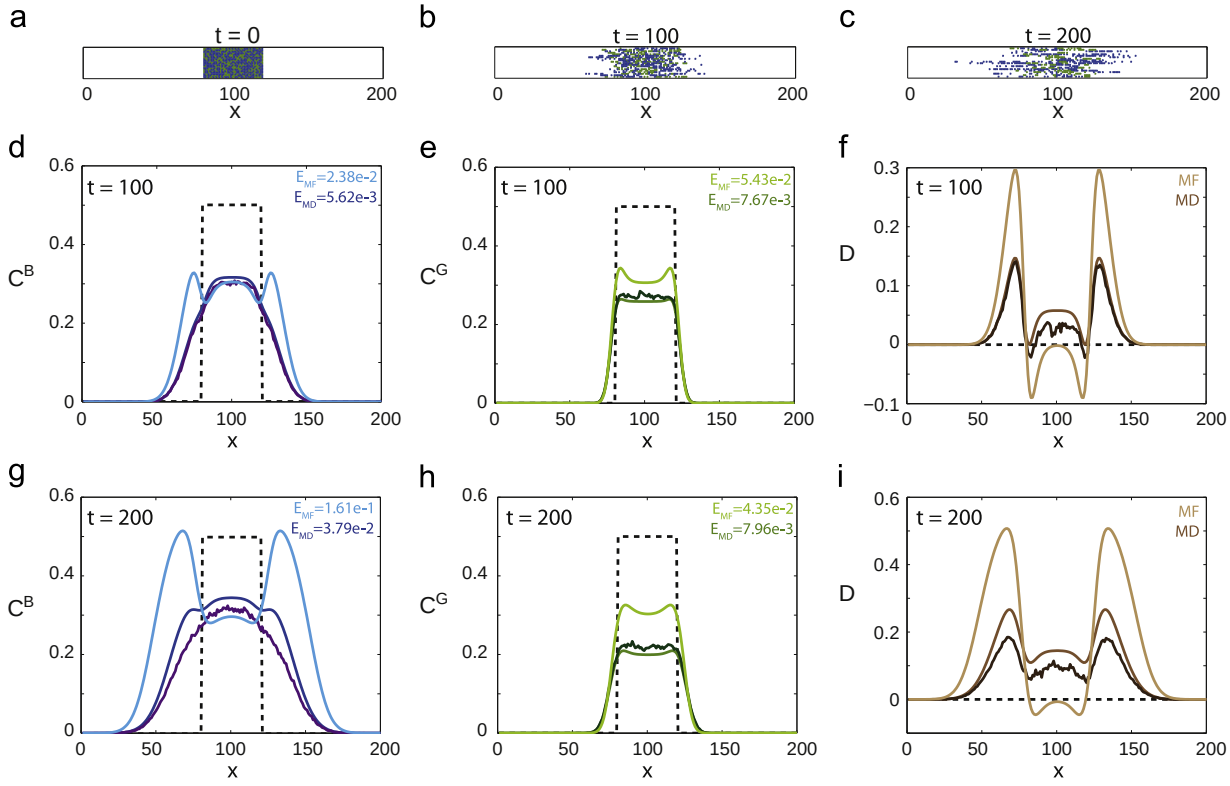

Fig. 2. One-dimensional model of a co-culture scratch assay. Snapshots of 20 identically prepared realisations of the discrete model at (a) $t=0$, (b) $t=100$ and (c) $t=200$. Comparison of the averaged discrete model (purple), traditional mean-field solution (light blue) and moment dynamics solution (blue) for cell subpopulation B at (d) $t=100$ and (g) $t=200$. Comparison of the averaged discrete model (dark green), traditional mean-field solution (light green) and moment dynamics solution (green) for cell subpopulation G at (e) $t=100$ and (h) $t=200$. Comparison of the averaged data from the discrete model (dark brown), traditional mean-field solution (light brown) and moment dynamics solution (brown) describing the difference in density, $D=C^B-C^G$, at (f) $t=100$ and (i) $t=200$. Parameters are $P_m^G=0.1$, $P_m^B=1$, $P_p^G=P_p^B=0.05$, $P_d^G=P_d^B=0.02$, $r_{\max}=100$, $C_0=0.5$, $\epsilon=10^{-8}$, $i_1=81$, $i_2=121$, $X=200$, $\Delta=1$. Averaged data from the discrete model corresponds to $M=10^4$ identically prepared realisations. In (d)–(i) the dashed lines correspond to initial condition, and the discrepancy between the averaged discrete density data and the solution of the traditional mean-field and the moment dynamics models, E_{MF} and E_{MD}, respectively, are given. (For interpretation of the references to colour in this figure caption, the reader is referred to the web version of this paper.)

In contrast, the moment dynamics model predicts the same qualitative behaviour as the averaged discrete model. The moment dynamics model provides a closer match to the averaged discrete data ($E_{\mathrm{MD}}=5.62\times10^{-3}$ for subpopulation B and 7.67×10^{-3} for subpopulation G) than the traditional mean-field approach ($E_{\mathrm{MF}}=2.38\times10^{-2}$ for subpopulation B and 5.43×10^{-2} for subpopulation G). An equivalent comparison between the averaged discrete data and the solutions of the traditional mean-field and moment dynamics models at $t=200$ is given in Fig. 2(g)–(i). Again, we observe that the traditional mean-field model predicts qualitatively different behaviour to the averaged discrete data, whereas the moment dynamics model provides a reasonable description of the averaged discrete data.

Since the key difference between the derivation of the mean-field model and the moment dynamics model is in the neglect of correlation effects, it is instructive to examine the magnitude of these differences. We can explore these differences since our numerical solution of the moment dynamics model produces estimates of $F_i^{G,G}(r\Delta)$, $F_i^{B,B}(r\Delta)$, $F_i^{G,B}(r\Delta)$ and $F_i^{B,G}(r\Delta)$ for $\Delta\le r\Delta\le r_{\max}\Delta$. Solution profiles showing $F_i^{G,G}(r\Delta)$, $F_i^{B,B}(r\Delta)$, $F_i^{G,B}(r\Delta)$ and $F_i^{B,G}(r\Delta)$ are given in the supplementary material document. Given that the mean-field model implicitly assumes that $F_i^{a,b}(r\Delta)\equiv1$ and that our solution profiles for $F_i^{G,G}(r\Delta)$, $F_i^{B,B}(r\Delta)$, $F_i^{G,B}(r\Delta)$ and $F_i^{B,G}(r\Delta)$ indicate that the correlation function is, at times, up to five orders of magnitude greater than unity, it is not surprising that the traditional mean-field model performs relatively poorly in this case.

The results in Fig. 2 correspond to one particular choice of the initial cell density in the scratch assay, and we now examine the sensitivity of the performance of the traditional mean-field model relative to the moment dynamics model by decreasing C_0, the initial density of the cell monolayer. We are interested to examine this sensitivity to initial density since previous studies have identified the initial density as playing a key role in the performance of these kinds of models (Baker and Simpson, 2010; Markham et al., 2013). Results in Fig. 3 are similar to those in Fig. 2 except that we consider a much lower initial density of cells by setting $C_0=0.1$ in Eq. (10). In general, we observe that the blue subpopulation in the discrete model moves further away from the initial condition with time than the green subpopulation, as shown in Fig. 3(a)–(c). Similar to the results in Fig. 2, the results in Fig. 3(d)–(i) show that the traditional mean-field model predicts qualitatively different behaviour than the averaged discrete density data in certain regions of the domain, while the moment dynamics model accurately captures the qualitative trends observed in the averaged discrete data. The details of the correlation functions for this problem are given in the supplementary material document.

To further investigate the performance of the moment dynamics model we now summarise results for a wider range of parameter combinations. Since the moment dynamics model requires additional effort to derive and solve compared to the traditional mean-field description, it is of interest to use our model to identify which particular parameter regimes require the application of a moment dynamics model, and which particular parameter regimes can be studied using the simpler traditional mean-field approach. Results in Table 1 describe the performance of the moment dynamics and traditional mean-field models for the same problem we considered in Fig. 2. Using criteria based on Eq. (9), we conclude that the moment dynamics model outperforms the traditional mean-field

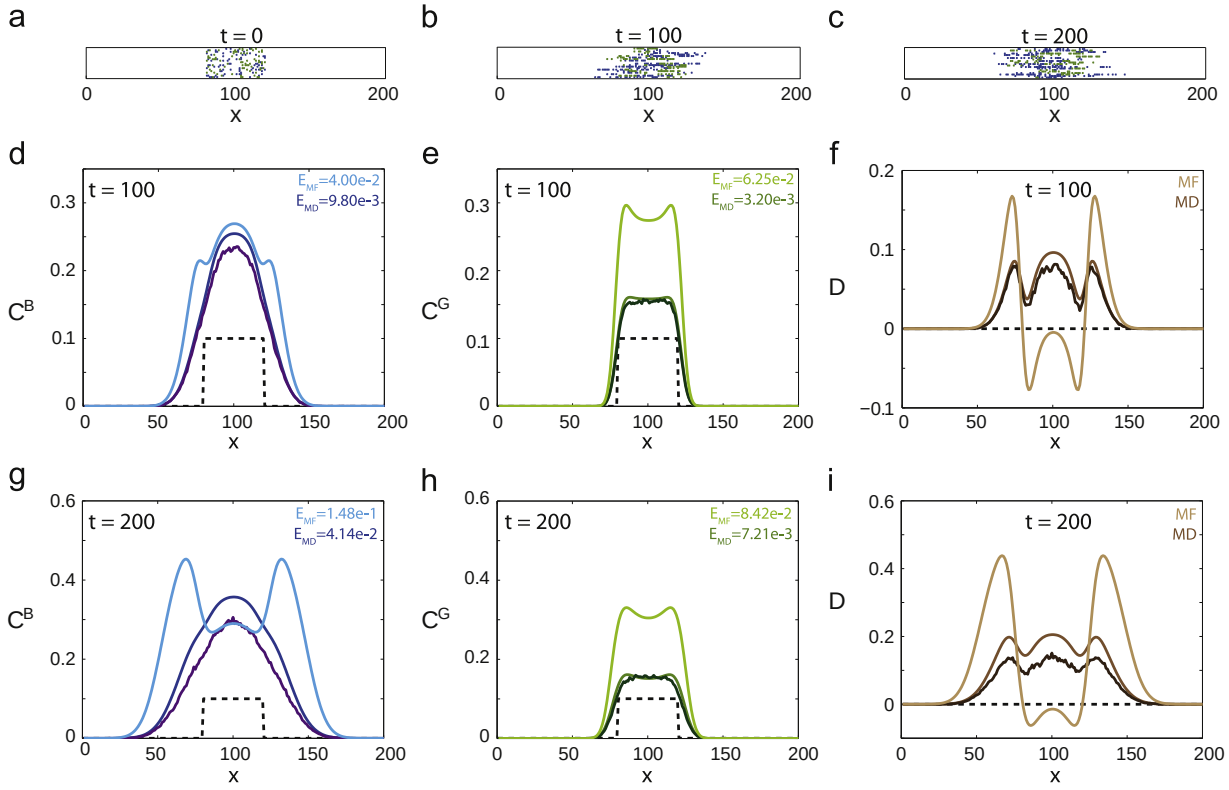

Fig. 3. One-dimensional model of a co-culture scratch assay. Snapshots of twenty identically prepared realisations of the discrete model at (a) $t=0$, (b) $t=100$ and (c) $t=200$. Comparison of the averaged discrete model (purple), traditional mean-field solution (light blue) and moment dynamics solution (blue) for subpopulation B at (d) $t=100$ and (g) $t=200$. Comparison of the averaged discrete model (dark green), traditional mean-field solution (light green) and moment dynamics solution (green) for subpopulation G at (e) $t=100$ and (h) $t=200$. Comparison of the averaged data from the discrete model (dark brown), traditional mean-field solution (light brown) and moment dynamics solution (brown) describing the difference in density, $D=C^B-C^G$, at (f) $t=100$ and (i) $t=200$. Parameters are $P_m^G=0.1$, $P_m^B=1$, $P_p^G=P_p^B=0.05$, $P_d^G=P_d^B=0.02$, $r_{\max}=100$, $C_0=0.1$, $\epsilon=10^{-8}$, $i_1=81$, $i_2=121$, $X=200$, $\Delta=1$. Averaged data from the discrete model corresponds to $M=10^4$ identically prepared realisations. In (d)–(i) the dashed lines correspond to initial condition, and the discrepancy between the averaged discrete density data and the solution of the traditional mean-field and the moment dynamics models, E_{MF} and E_{MD}, respectively, are given. (For interpretation of the references to colour in this figure caption, the reader is referred to the web version of this paper.)

Table 1
Parameter ratios and the validity of both the mean-field and moment dynamics models for describing the averaged discrete model for those parameter ratios and the cell co-culture scratch assay initial condition. Large indicates 10^1 or higher, intermediate indicates 5×10^{-2}–5×10^{0}, small indicates less than 10^{-2}. **X** denotes a model that is inappropriate for the corresponding parameter ratio while **X*** denotes a model that provides an accurate prediction for one subpopulation, but not both. The tick symbol denotes a model that provides a prediction that matches the averaged discrete model well.

P_m^B/P_m^G	P_p^B/P_p^G	P_d^B/P_d^G	P_p^B/P_m^B	P_p^G/P_m^G	P_d^B/P_p^B	P_d^G/P_p^G	Mean-field	Corrected mean-field
Large	Intermediate	Intermediate	Intermediate	Intermediate	Intermediate	Intermediate	**X**	✓
Intermediate	Intermediate	Intermediate	Intermediate	Intermediate	Intermediate	Large	**X***	✓
Large	Large	Intermediate	Small	Small	Intermediate	Large	✓	✓
Intermediate	Intermediate	Large	Intermediate	Intermediate	Intermediate	Small	**X***	✓
Intermediate	Intermediate	Intermediate	Small	Small	Large	Large	✓	✓
Intermediate	Intermediate	Intermediate	Large	Large	Intermediate	Intermediate	**X**	✓
Large	Intermediate	Intermediate	Small	Large	Intermediate	Intermediate	**X***	✓

description across a large range of parameter combinations. In particular, we observe that the traditional mean-field model fails to describe the average behaviour of the discrete model whenever proliferation is significant, that is, where the proliferation rate is not significantly smaller than the motility rate. We observe that if, for both subpopulations, P_p^k is small compared to P_m^k, then the mean-field model describes the averaged discrete model well for both subpopulations. While the mean-field model is appropriate in certain parameter regimes, the moment dynamics model always provides an improved match to the averaged discrete density data.

3.1.2. *Two-dimensional co-culture stencil assay*

We now present results for a two-dimensional extension of the model considered in Section 3.1.1. While we motivated the geometry of our simulations in Section 3.1.1 by considering a scratch assay, we note that there are several other types of *in vitro* assays, such as barrier assays (Simpson et al., 2013) or stencil assays (Kroening and Goppelt-Struebe, 2010; Riahi et al., 2012), that involve an initially confined population of cells which spread in two dimensions. The details of the equations governing the two-dimensional moment dynamics model are given in the supplementary material document. We apply our model to a square stencil assay, where cells are grown initially inside a square stencil. The assay is initiated by removing the stencil and allowing the cells to spread into the area surrounding the initially confined population of cells. We model this process using an initial condition given by

$$C_{(i,j)}^G(0)=C_{(i,j)}^B(0)=\begin{cases} C_0, & i_1\le i<i_2, j_1\le j<j_2,\\ \epsilon & \text{elsewhere.}\end{cases} \tag{11}$$

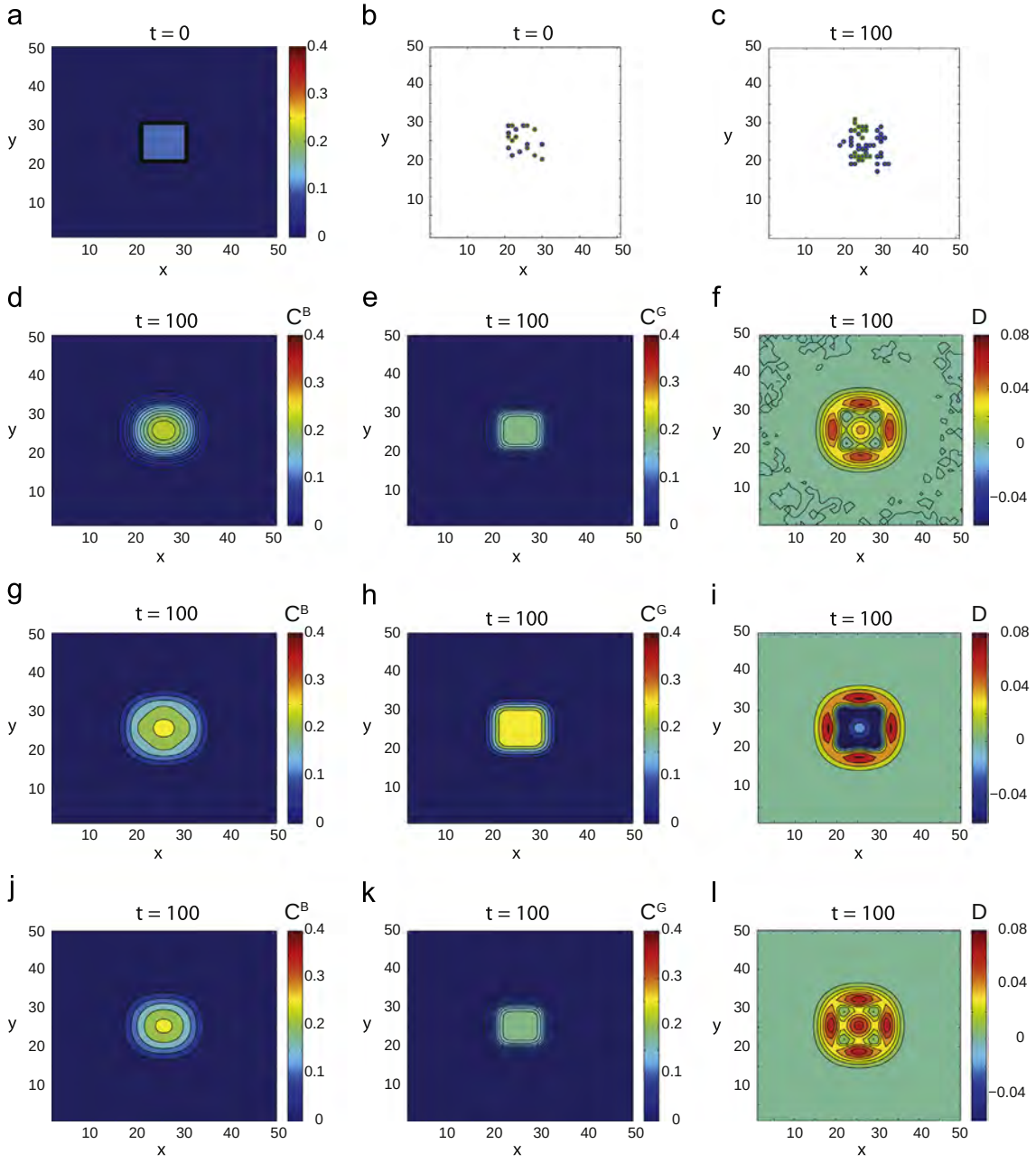

Fig. 4. Two-dimensional model of a co-culture stencil assay. (a) Initial condition for the traditional mean-field and moment dynamics model. Single realisation of the discrete model at (b) $t=0$ and (c) $t=100$. Averaged density data from the discrete model for (d) subpopulation B and (e) subpopulation G at $t=100$. (f) Averaged data from the discrete model describing the difference between the two subpopulations, $D=C^B-C^G$. Traditional mean-field solution for (g) subpopulation B and (h) subpopulation G at $t=100$. (i) Difference between the two subpopulations, $D=C^B-C^G$, for the traditional mean-field model. Corrected mean-field solution for (j) subpopulation B and (k) subpopulation G at $t=100$. (i) Difference between the two subpopulations, C^B-C^G, for the moment dynamics model. Parameters are $P_m^G=0.01$, $P_m^B=0.1$, $P_p^G=P_p^B=0.05$, $P_d^G=P_d^B=0.02$, $r_{\max}=5$, $C_0=0.1$, $\epsilon=10^{-8}$, $i_1=j_1=81$, $i_2=j_2=121$, $X=Y=50$. Difference, given by Eq. (9), between the mean-field solution and the averaged discrete model: 1.57×10^{-2} (subpopulation B) and 2.49×10^{-2} (subpopulation G). Averaged data from the discrete model corresponds to $M=10^6$ identically prepared realisations. The discrepancy between the averaged discrete density data and the solution of the traditional mean-field and the moment dynamics models, given by Eq. (9) are (d) 3.90×10^{-3} (subpopulation B) and 9.48×10^{-4} (subpopulation G).

Again, we make the assumption that both cell subpopulations are initially present at the same density, such as the traditional mean-field initial condition shown in Fig. 4(a) with both subpopulations present with $C_0=0.1$ inside the square stencil. The discrete analogue of this initial condition for a single realisation of the discrete model is presented in Fig. 4(b). We allow the discrete model to evolve until $t=100$, and present a snapshot of the results in Fig. 4(c). In the two-dimensional setting we observe the formation of clustering, particularly in the less motile G subpopulation. This kind of clustering is frequently observed in many different experimental situations, such as in Fig. 1(c).

We perform many identically prepared realisations of the discrete model and present the average density distributions, for both subpopulation B and subpopulation G, in Fig. 4(d) and (e), respectively. As we might expect, the more motile subpopulation B spreads further away from the location of the initial condition than subpopulation G. Interestingly, although both cell subpopulations have the same rates of proliferation and death, subpopulation B has a

higher maximum density. The difference between the density of the two subpopulations is reported in Fig. 4(f) and we observe that, aside from minor fluctuations, we have $C^B_{(i,j)} > C^G_{(i,j)}$ across the domain. It is instructive to examine whether this qualitative behaviour is captured by the traditional mean-field and moment dynamics models. The traditional mean-field solutions for subpopulations B and G, presented in Fig. 4(g) and (h), respectively, exhibit higher cell density than the averaged discrete data. In particular, according to the traditional mean-field model, subpopulation G has a maximum density of approximately 0.25 whereas the maximum density according to the averaged data from the discrete model is approximately 0.15. The difference between the density of the two subpopulations according to the traditional mean-field model, given in Fig. 4(i), predicts that $C^G_{(i,j)} > C^B_{(i,j)}$ in large parts of the domain, which is precisely the opposite of what we observe in the averaged discrete data.

To investigate whether including spatial correlation addresses the limitations of the traditional mean-field model, we compare the predictions of our moment dynamics model with the averaged discrete model. We note that, in the two-dimensional case, lattice sites separated in both the x and y directions can be correlated and that the maximum separation in both the x and y directions is denoted by $r_{\max}$. The relevant solution of the moment dynamics model is presented in Fig. 4(j) and (k) for subpopulations B and G, respectively. Visually, we observe that the moment dynamics model matches the averaged discrete data far better than the solution of the traditional mean-field model. Indeed, measuring the difference between the solution of the moment dynamics model and the averaged discrete data leads to estimates of E_{MD} that are approximately one order of magnitude lower than estimates of E_{MF}.

3.2. Case study 2: invasion of one subpopulation into another subpopulation

Cell invasion occurs when one cell subpopulation moves through a distinct background cell subpopulation, such as tumour cells spreading through the stroma (Bhowmick and Moses, 2005). To model this kind of process we assume that the background cell subpopulation is initially spatially uniform and can be modelled as a one-dimensional process. Therefore, we assume that one cell subpopulation, C^G_i, is uniformly distributed at some initial density, C^G_0, while the other cell subpopulation is initially confined, so that we can mimic the kind of geometry we see in Fig. 1(d). To achieve this we set

$$C^G_i(0) = C^G_0, \quad 1 \le i \le X,$$
$$C^B_i(0) = \begin{cases} \epsilon, & 1 \le i < i_1, \\ C^B_0, & i_1 \le i < i_2, \\ \epsilon, & i_2 \le i \le X, \end{cases} \tag{12}$$

as the initial condition, where $\epsilon \ll 1$.

Twenty identically prepared realisations of the one-dimensional discrete model, at $t=0$, $t=100$ and $t=200$, are presented in Figs. 5(a)–(c) and 6(a)–(c), respectively. The difference between Figs. 5 and 6 is in the choice of parameters. In summary, subpopulation B is more motile than subpopulation G in Fig. 5, whereas subpopulation G is more motile than subpopulation B in Fig. 6. We compare the relative performance of the traditional mean-field and moment dynamics models for the relevant parameter choices in Figs. 5(d)–(f) and 6(d)–(f) at $t=100$, and in Figs. 5(g)–(i) and 6(g)–(i) at $t=200$. In general, we

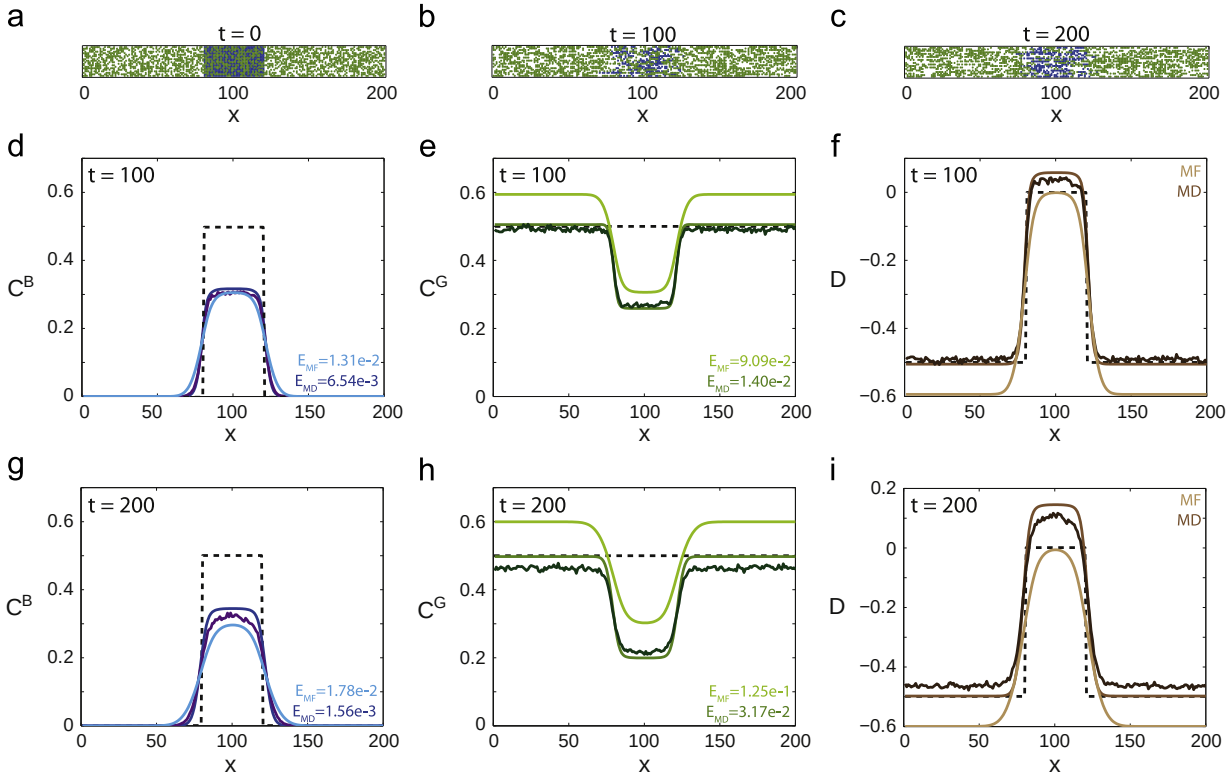

Fig. 5. One-dimensional model of cell invasion. Snapshots of 20 identically prepared realisations of the discrete model at (a) $t=0$, (b) $t=100$ and (c) $t=200$. Comparison of the averaged discrete model (purple), corresponding mean-field solution (light blue) and moment dynamics solution (blue) for cell subpopulation B at (d) $t=100$ and (g) $t=200$. Comparison of the averaged discrete model (dark green), corresponding mean-field solution (light green) and moment dynamics solution (green) for cell subpopulation G at (e) $t=100$ and (h) $t=200$. Comparison of the averaged discrete model (dark brown), corresponding mean-field solution (light brown) and moment dynamics solution (brown) for the difference in cell subpopulations $D = C^B - C^G$ at (f) $t=100$ and (i) $t=200$. Parameters are $P^G_m = 0.1$, $P^B_m = 1$, $P^G_p = P^B_p = 0.05$, $P^G_d = P^B_d = 0.02$, $r_{\max} = 100$, $C^G_0 = C^B_0 = 0.5$, $\epsilon = 10^{-8}$, $i_1 = 81$, $i_2 = 121$, $X = 200$, $\Delta = 1$. Averaged data from the discrete model corresponds to $M = 10^4$ identically prepared realisations. In (d)–(i) the dashed lines correspond to initial condition, and the discrepancy between the averaged discrete density data and the solution of the traditional mean-field and the moment dynamics models, E_{MF} and E_{MD}, respectively, are given. (For interpretation of the references to colour in this figure caption, the reader is referred to the web version of this paper.)

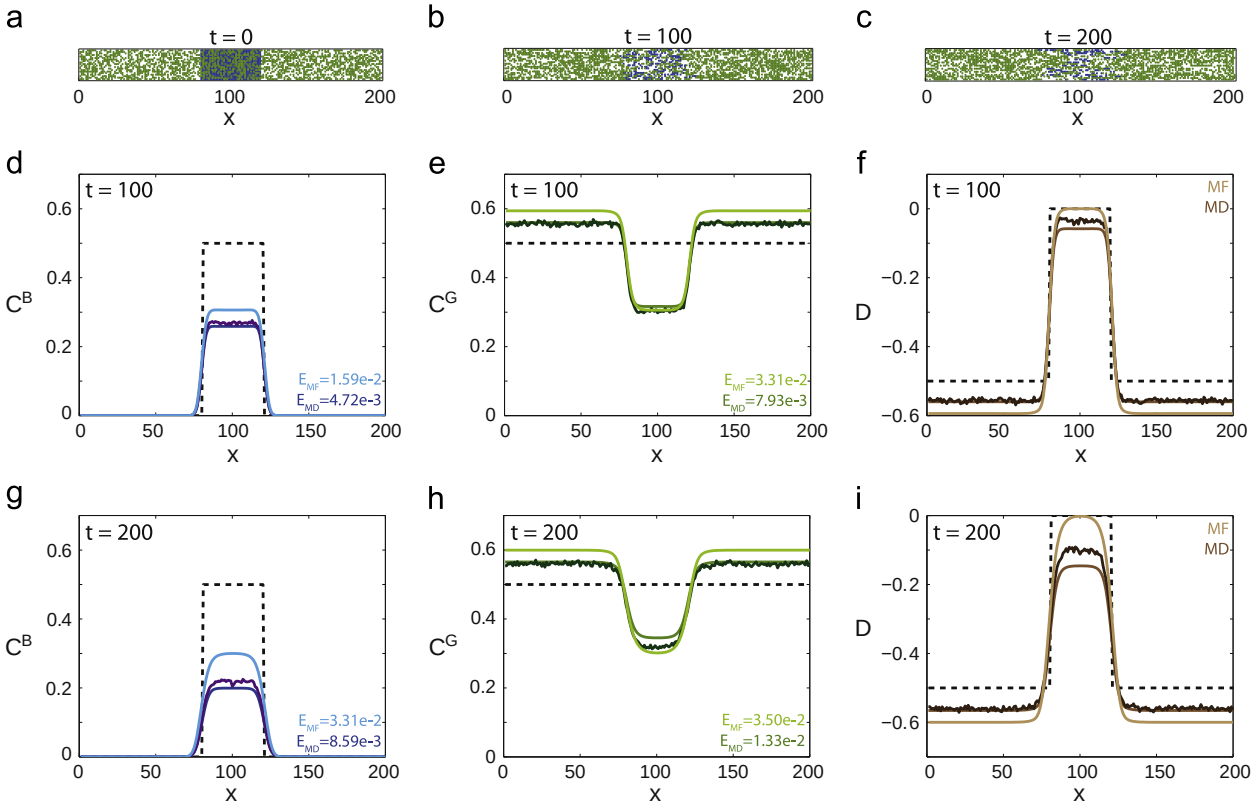

Fig. 6. One-dimensional model of cell invasion. Snapshots of 20 identically prepared realisations of the discrete model at (a) $t=0$, (b) $t=100$ and (c) $t=200$. Comparison of the averaged discrete model (purple), corresponding mean-field solution (light blue) and moment dynamics solution (blue) for cell subpopulation B at (d) $t=100$ and (g) $t=200$. Comparison of the averaged discrete model (dark green), corresponding mean-field solution (light green) and moment dynamics solution (green) for cell subpopulation G at (e) $t=100$ and (h) $t=200$. Comparison of the averaged discrete model (dark brown), corresponding mean-field solution (light brown) and moment dynamics solution (brown) for the difference in cell subpopulations $D=C^B-C^G$, at (f) $t=100$ and (i) $t=200$. Parameters are $P_m^G=1$, $P_m^B=0.1$, $P_p^G=P_p^B=0.05$, $P_d^G=P_d^B=0.02$, $r_{\max}=100$, $C_0^G=C_0^B=0.5$, $\epsilon=10^{-8}$, $i_1=81$, $i_2=121$, $X=200$, $\Delta=1$. Averaged data from the discrete model corresponds to $M=10^4$ identically prepared realisations. In (d)–(i) the dashed lines correspond to initial condition, and the discrepancy between the averaged discrete density data and the solution of the traditional mean-field and the moment dynamics models, E_{MF} and E_{MD}, respectively, are given. (For interpretation of the references to colour in this figure caption, the reader is referred to the web version of this paper.)

observe that the solution of the moment dynamics model provides an improved match to the averaged discrete data relative to the solution of the traditional mean-field model for both parameter choices. In particular, the solution of the moment dynamics model provides an improved approximation of the averaged density from the discrete model at the low density leading edge of the invading subpopulation in Fig. 5 where $P_m^B > P_m^G$. This improvement offered by the moment dynamics model at the leading edge of the spreading population is of particular interest when considering surgical removal of tumours where it is essential to have a good understanding of the location of the leading edge of the spreading subpopulation (Beets-Tan et al., 2001; Swan, 1975).

To examine the role of initial cell density we present an additional set of results in Fig. 7 where we have reduced the initial cell density. The additional results in Fig. 7 involve the same initial conditions, given by Eq. (12), except that we set $C_0^G=C_0^B=0.1$. Since the background density has been decreased, we observe that the invading subpopulation spreads further in Fig. 7 than in the corresponding situations presented in Figs. 5 and 6. It is interesting that both the solutions of the mean-field and moment dynamics models are less accurate in describing the density of the background subpopulation for the lower density initial condition.

To provide more comprehensive insight into the relative performance of the moment dynamics model we also examine the match between the average density data and the solution of the traditional mean-field and the moment dynamics models over a range of parameter combinations. The results of this comparison are summarised in Table 2, where we see that the solution of the moment dynamics model matches the averaged density data from the discrete model better than the corresponding solution of the traditional mean-field model in each parameter regime considered. We also observe that the traditional mean-field model is appropriate for situations where the proliferation rate is small relative to the motility rate.

4. Discussion and conclusions

In this work we have considered developing mathematical models which describe the motion of populations containing distinct subpopulations. These kinds of processes are relevant to a range of biological and ecological applications including malignant spreading (Sherratt, 2000), wound healing (Sherratt and Murray, 1990) and the spread of invasive species (Hastings et al., 2005). Previous models of these processes typically focus on population-level PDE descriptions that neglect to explicitly account for individual-level behaviour (Gatenby and Gawlinski, 1996; Painter and Sherratt, 2003; Sherratt, 2000; Smallbone et al., 2005). To partly address this limitation, other researchers use discrete mathematical models in conjunction with the associated population-level PDE description which is derived from the underlying stochastic process by invoking a mean-field approximation (Khain et al., 2012; Simpson et al., 2010). While averaged density data from these kinds of stochastic models is known to match the solution of the associated mean-field PDE approximation in certain parameter regimes, it is well-known that mean-field PDE descriptions fail to match average density information from the stochastic process for

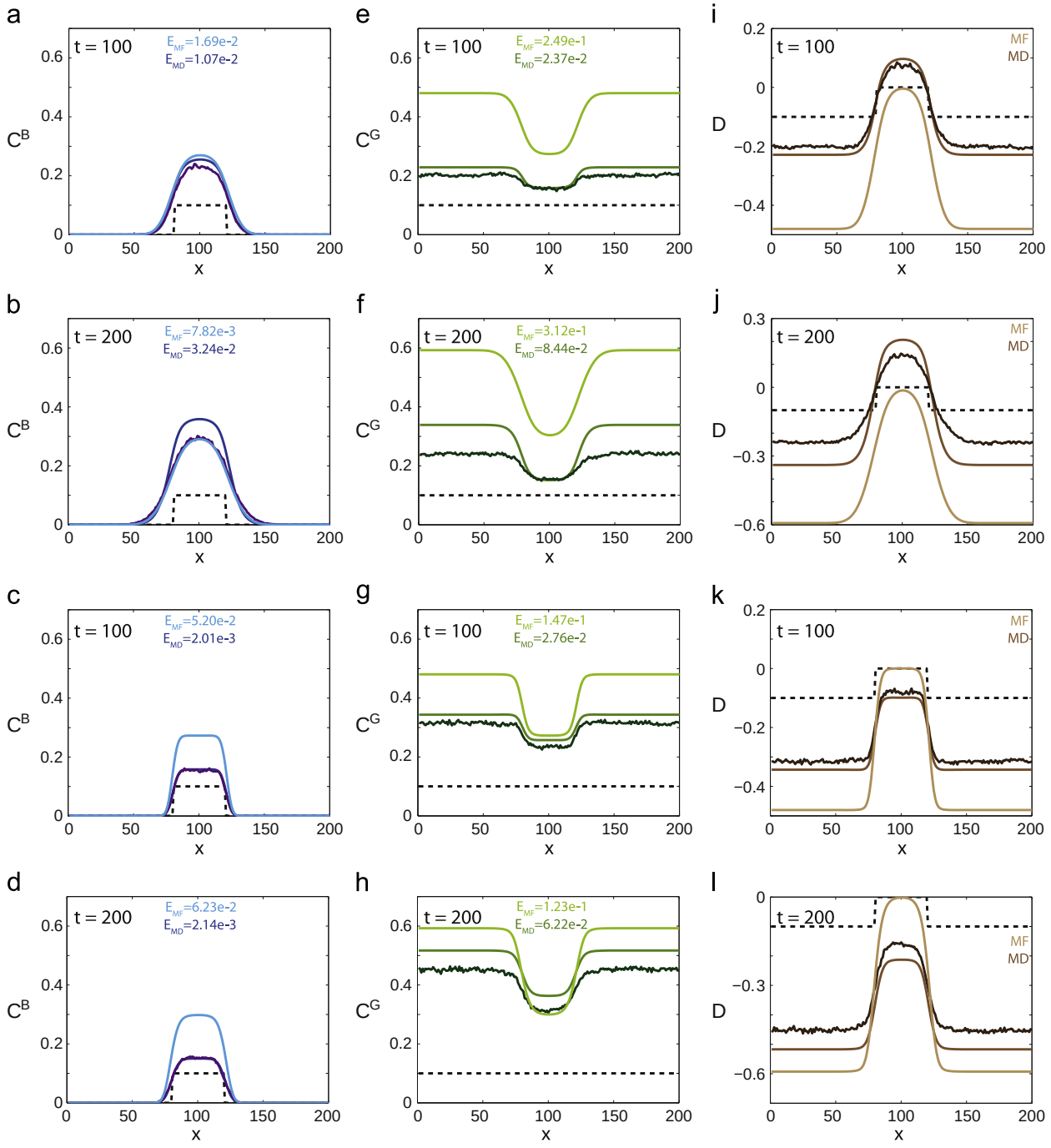

Fig. 7. One-dimensional model of cell invasion. Comparison of the averaged discrete model (purple), corresponding mean-field solution (light blue) and moment dynamics solution (blue) for cell subpopulation B at (a), (c) $t=100$ and (b), (d) $t=200$ for (a), (b) parameter regime one and (c), (d) parameter regime two. Comparison of the averaged discrete model (purple), corresponding mean-field solution (light blue) and moment dynamics solution (blue) for cell subpopulation G at (e), (g) $t=100$ and (f), (h) $t=200$ for (e), (f) parameter regime one and (g), (h) parameter regime two. Comparison of the averaged discrete model (purple), corresponding mean-field solution (light blue) and moment dynamics solution (blue) for cell subpopulation $D=C^B-C^G$, at (i), (k) $t=100$ and (j), (l) $t=200$ for (i), (j) parameter regime one and (k), (l) parameter regime two. Parameters used were $r_{\max}=100$, $C_0^G=C_0^B=0.1$, $\epsilon=10^{-8}$, $i_1=81$, $i_2=121$, $X=200$, $\Delta=1$. Parameter regime one used $P_m^G=0.1$, $P_m^B=1$, $P_p^G=P_p^B=0.05$, $P_d^G=P_d^B=0.02$. Parameter regime two used $P_m^G=1$, $P_m^B=0.1$, $P_p^G=P_p^B=0.05$, $P_d^G=P_d^B=0.02$. Averaged data from the discrete model corresponds to $M=10^4$ identically prepared realisations. In (a)–(l) the dashed lines correspond to initial condition, and the discrepancy between the averaged discrete density data and the solution of the traditional mean-field and the moment dynamics models, E_{MF} and E_{MD}, respectively, are given. (For interpretation of the references to colour in this figure caption, the reader is referred to the web version of this paper.)

parameter combinations where the discrete model leads to significant correlation and clustering effects (Baker and Simpson, 2010).

Our study, in which we derive new moment dynamics models governing the motion of cell populations composed of interacting subpopulations, offers two improvements on previous approaches. First, our moment dynamics model approximately incorporates clustering and correlation, which are implicitly neglected in previous PDE-based descriptions. This is important since clustering and correlation effects are often observed in cell biology experiments (Treloar et al., 2014). We note that the clustering incorporated is not due to explicit cell-to-cell adhesion but from the nature of the proliferation mechanism. Second, our moment dynamics model is more computationally efficient to implement than using a large number of repeated stochastic realisations of the discrete model. By presenting a thorough comparison of

Table 2
Parameter ratios and the validity of the mean-field and moment dynamics models for describing the averaged discrete model for the cell invasion initial condition. Large indicates 10^1 or higher, intermediate indicates 5×10^{-2}–5×10^{0}, small indicates less than 10^{-2}. **X** denotes a model that is inappropriate for the corresponding parameter ratio while **X*** denotes a model that provides an accurate prediction for one subpopulation, but not both. The tick symbol denotes a model that matches the averaged discrete model well.

P_m^B/P_m^G	P_p^B/P_p^G	P_d^B/P_d^G	P_p^B/P_m^B	P_p^G/P_m^G	P_d^B/P_p^B	P_d^G/P_p^G	Mean-field	Corrected mean-field
Large	Intermediate	Intermediate	Intermediate	Intermediate	Intermediate	Intermediate	**X**	✓
Intermediate	Large	Intermediate	Intermediate	Intermediate	Intermediate	Large	**X**	✓
Intermediate	Intermediate	Intermediate	Intermediate	Intermediate	Intermediate	Large	**X***	✓
Large	Large	Intermediate	Small	Small	Intermediate	Large	**X***	✓
Intermediate	Intermediate	Intermediate	Small	Small	Intermediate	Intermediate	✓	✓
Intermediate	Intermediate	Intermediate	Intermediate	Intermediate	Small	Intermediate	**X**	✓
Intermediate	Intermediate	Intermediate	Small	Small	Large	Large	**X***	✓
Intermediate	Intermediate	Intermediate	Large	Large	Intermediate	Intermediate	**X***	✓
Large	Intermediate	Intermediate	Small	Large	Intermediate	Intermediate	**X**	✓
Small	Large	Intermediate	Large	Small	Intermediate	Intermediate	**X***	✓

the performance of a traditional mean-field model and the new moment dynamics model for two case studies we are able to summarise some of the general features of our model. While we always find that the moment dynamics model produces a more accurate description of the entire cell density profile than the traditional mean-field model, we also find that certain features of the processes are reliably predicted by the traditional mean-field framework.

There are several ways that our work could be extended. In all cases we always assume that the influence of cell-to-cell adhesion and cell-to-substrate adhesion is negligible. While these assumptions are relevant for certain types of cells, it is well known that other types of cells, such as glioma and melanoma, exhibit significant adhesion (Khain et al., 2012; Treloar and Simpson, 2013; Treloar et al., 2014). Therefore, it is of interest to examine how to incorporate the effects of cell-to-cell adhesion and cell-to-substrate adhesion in our moment dynamics framework. In this work we have only considered cell biology as an application of this framework. Future applications of this framework could include chemical kinetics (Singh and Hespanha, 2011) and predator–prey interactions (Murrell, 2005). A further extension would be to consider an off-lattice discrete process, such as the model presented by Middleton et al. (2014). Given that off-lattice discrete models are far more computationally expensive than lattice-based discrete models, the need for efficient and accurate mean-field descriptions of these processes is even more significant for off-lattice models than for lattice-based models. We leave these extensions for future analysis.

Acknowledgements

This work was financially supported by the Cooperative Research Centre for Wound Management Innovation and the Australian Research Council (FT130100148). We also appreciate the assistance of Emeritus Professor Sean McElwain.

Appendix A. Supplementary data

Supplementary data associated with this paper can be found in the online version at http://dx.doi.org/10.1016/j.jtbi.2015.01.025.

References

Baker, R.E., Simpson, M.J., 2010. Correcting mean-field approximations for birth–death-movement processes. Phys. Rev. E 82 (4), 041905.
Beets-Tan, R., Beets, G., Vliegen, R., Kessels, A., Van Boven, H., De Bruine, A., Von Meyenfeldt, M., Baeten, C., Van Engelshoven, J., 2001. Accuracy of magnetic resonance imaging in prediction of tumour-free resection margin in rectal cancer surgery. The Lancet 357 (9255), 497–504.
Bhowmick, N.A., Moses, H.L., 2005. Tumor–stroma interactions. Curr. Opin. Genet. Dev. 15 (1), 97–101.
Binder, B.J., Landman, K.A., 2009. Exclusion processes on a growing domain. J. Theor. Biol. 259 (3), 541–551.
Chowdhury, D., Schadschneider, A., Nishinari, K., 2005. Physics of transport and traffic phenomena in biology: from molecular motors and cells to organisms. Phys. Life Rev. 2 (4), 318–352.
Codling, E.A., Plank, M.J., Benhamou, S., 2008. Random walk models in biology. J. R. Soc. Interface 5 (25), 813–834.
De Wever, O., Mareel, M., 2003. Role of tissue stroma in cancer cell invasion. J. Pathol. 200 (4), 429–447.
Fernando, A.E., Landman, K.A., Simpson, M.J., 2010. Nonlinear diffusion and exclusion processes with contact interactions. Phys. Rev. E 81 (1), 011903.
Gatenby, R.A., Gawlinski, E.T., 1996. A reaction–diffusion model of cancer invasion. Cancer Res. 56 (24), 5745–5753.
Gatenby, R.A., Gawlinski, E.T., Gmitro, A.F., Kaylor, B., Gillies, R.J., 2006. Acid-mediated tumor invasion: a multidisciplinary study. Cancer Res. 66 (10), 5216–5223.
Gillespie, D.T., 1977. Exact stochastic simulation of coupled chemical reactions. J. Phys. Chem. 81 (25), 2340–2361.
Grima, R., 2008. Multiscale modeling of biological pattern formation. Curr. Top. Dev. Biol. 81, 435–460.
Hastings, A., Cuddington, K., Davies, K.F., Dugaw, C.J., Elmendorf, S., Freestone, A., Harrison, S., Holland, M., Lambrinos, J., Malvadkar, U., et al., 2005. The spatial spread of invasions: new developments in theory and evidence. Ecol. Lett. 8 (1), 91–101.
Johnston, S.T., Simpson, M.J., Baker, R.E., 2012. Mean-field descriptions of collective migration with strong adhesion. Phys. Rev. E 85 (5), 051922.
Khain, E., Katakowski, M., Charteris, N., Jiang, F., Chopp, M., 2012. Migration of adhesive glioma cells: front propagation and fingering. Phys. Rev. E 86 (1), 011904.
Kroening, S., Goppelt-Struebe, M., 2010. Analysis of matrix-dependent cell migration with a barrier migration assay. Sci. Signal. 3 (126), pl1.
Law, R., Dieckmann, U., 2000. A dynamical system for neighborhoods in plant communities. Ecology 81 (8), 2137–2148.
Li, G., Satyamoorthy, K., Meier, F., Berking, C., Bogenrieder, T., Herlyn, M., 2003. Function and regulation of melanoma–stromal fibroblast interactions: when seeds meet soil. Oncogene 22 (20), 3162–3171.
Markham, D.C., Simpson, M.J., Maini, P.K., Gaffney, E.A., Baker, R.E., 2013. Incorporating spatial correlations into multispecies mean-field models. Phys. Rev. E 88 (5), 052713.
Middleton, A.M., Fleck, C., Grima, R., 2014. A continuum approximation to an off-lattice individual-cell based model of cell migration and adhesion. J. Theor. Biol. 359, 220–232.
Murrell, D.J., 2005. Local spatial structure and predator–prey dynamics: counter-intuitive effects of prey enrichment. Am. Nat. 166 (3), 354–367.
Oberringer, M., Meins, C., Bubel, M., Pohlemann, T., 2007. A new in vitro wound model based on the co-culture of human dermal microvascular endothelial cells and human dermal fibroblasts. Biol. Cell 99 (4), 197–207.
Painter, K.J., Sherratt, J.A., 2003. Modelling the movement of interacting cell populations. J. Theor. Biol. 225 (3), 327–339.
Phillips, B.L., Brown, G.P., Greenlees, M., Webb, J.K., Shine, R., 2007. Rapid expansion of the cane toad (*Bufo marinus*) invasion front in tropical Australia. Austral Ecol. 32 (2), 169–176.
Riahi, R., Yang, Y., Zhang, D.D., Wong, P.K., 2012. Advances in wound-healing assays for probing collective cell migration. J. Lab. Autom. 17 (1), 59–65.
Shampine, L.F., Reichelt, M.W., 1997. The Matlab ODE suite. SIAM J. Sci. Comput. 18 (1), 1–22.
Sherratt, J.A., 2000. Wavefront propagation in a competition equation with a new motility term modelling contact inhibition between cell populations. Proc. R. Soc. Lond. Ser. A: Math. Phys. Eng. Sci. 456(2002), 2365–2386.
Sherratt, J.A., Murray, J., 1990. Models of epidermal wound healing. Proc. R. Soc. Lond. Ser. B: Biol. Sci. 241(1300), 29–36.
Simpson, M.J., Baker, R.E., 2011. Corrected mean-field models for spatially dependent advection–diffusion–reaction phenomena. Phys. Rev. E 83 (5), 051922.

Simpson, M.J., Haridas, P., McElwain, D.L.S., 2014. Do pioneer cells exist? PloS One 9 (1), e85488.
Simpson, M.J., Landman, K.A., Bhaganagarapu, K., 2007a. Coalescence of interacting cell populations. J. Theor. Biol. 247 (3), 525–543.
Simpson, M.J., Landman, K.A., Hughes, B.D., 2009. Multi-species simple exclusion processes. Physica A: Stat. Mech. Appl. 388 (4), 399–406.
Simpson, M.J., Landman, K.A., Hughes, B.D., 2010. Cell invasion with proliferation mechanisms motivated by time-lapse data. Physica A: Stat. Mech. Appl. 389 (18), 3779–3790.
Simpson, M.J., Treloar, K.K., Binder, B.J., Haridas, P., Manton, K.J., Leavesley, D.I., McElwain, D.L.S., Baker, R.E., 2013. Quantifying the roles of cell motility and cell proliferation in a circular barrier assay. J. R. Soc. Interface 10 (82), 20130007.
Simpson, M.J., Zhang, D.C., Mariani, M., Landman, K.A., Newgreen, D.F., 2007b. Cell proliferation drives neural crest cell invasion of the intestine. Dev. Biol. 302 (2), 553–568.
Singer, A., 2004. Maximum entropy formulation of the Kirkwood superposition approximation. J. Chem. Phys. 121 (8), 3657–3666.
Singh, A., Hespanha, J.P., 2011. Approximate moment dynamics for chemically reacting systems. IEEE Trans. Autom. Control 56 (2), 414–418.
Skellam, J., 1951. Random Dispersal in Theoretical PopulationsBiometrika196–218
Smallbone, K., Gavaghan, D.J., Gatenby, R.A., Maini, P.K., 2005. The role of acidity in solid tumour growth and invasion. J. Theor. Biol. 235 (4), 476–484.
Swan, G.W., 1975. A mathematical model for the density of malignant cells in the spread of cancer in the uterus. Math. Biosci. 25 (3), 319–329.
Treloar, K.K., Simpson, M.J., 2013. Sensitivity of edge detection methods for quantifying cell migration assays. PLoS One 8 (6), e67389.
Treloar, K.K., Simpson, M.J., Binder, B.J., McElwain, D.L.S., Baker, R.E., 2014. Assessing the role of spatial correlations during collective cell spreading. Sci. Rep. 4 (5713).
Walter, M., Wright, K.T., Fuller, H., MacNeil, S., Johnson, W.E.B., 2010. Mesenchymal stem cell-conditioned medium accelerates skin wound healing: an in vitro study of fibroblast and keratinocyte scratch assays. Exp. Cell Res. 316 (7), 1271–1281.